J|A|C|S ARTICLES

Published on Web 07/22/2009

Triplet Excimer Formation in Platinum-Based Phosphors: A Theoretical Study of the Roles of Pt−Pt Bimetallic Interactions and Interligand $\pi-\pi$ Interactions

Dongwook Kim and Jean-Luc Brédas*

School of Chemistry and Biochemistry and Center for Organic Photonics and Electronics, Georgia Institute of Technology, Atlanta, Georgia 30332-0400

Received December 19, 2008; E-mail: jean-luc.bredas@chemistry.gatech.edu

Abstract: We have used density functional theory (DFT) and time-dependent DFT to investigate the geometric and electronic structure and the optical properties of the phosphorescent platinum compounds: Pt(II) (2-(4′,6′-difluorophenyl)pyridinato-*N*,$C^{2'}$)(2,4-pentanedionato-*O*,*O*) (FPt1) and Pt(II) (2-(4′,6′-difluorophenyl)pyridinato-*N*,$C^{2'}$)(1,3-propanedionato-*O*,*O*) (FPt0). We first examined isolated compounds (monomers) and evaluated their photophysical properties at the ground-state and lowest triplet excited-state (T_1) geometries; the characteristics of the $S_0 \rightarrow T_1$ transitions are nearly identical in both compounds. Dimers of FPt0 and of FPt1 were then studied in order to shed light, at least qualitatively, on the respective role of Pt−Pt bimetallic interactions and interligand $\pi-\pi$ interactions in the formation of excimer structures. While the Pt−Pt interactions are critical for excimer formation, the interligand $\pi-\pi$ interactions also play a significant role in determining the optimal excimer geometry and the magnitude of the phosphorescence energy lowering in going from the monomer to the aggregated dimer. The distorted cofacial-type excimer structures found for FPt1, with a Pt−Pt distance around 2.9 Å and interligand distances around 3.5−3.8 Å, lead to phosphorescence energy lowerings with respect to the monomer on the order of 0.7−0.96 eV, in very good agreement with experiment.

1. Introduction

Since the seminal works of Tang and co-workers[1] and Friend and co-workers[2] on efficient electroluminescence (EL) in organic small molecules and polymers, organic-light emitting diodes (OLEDs) have attracted an enormous interest[3] due to their strong potential for applications in display and lighting technologies. In particular, white OLEDs (WOLEDs) are being intensively investigated as a promising alternative to incandescent or fluorescent lamps.[4] In a WOLED, three colors (red, green, and blue) or two colors (such as orange and blue) must be emitted simultaneously to generate white light. Since the use of different emitters and emitting layers adds to the complexity of the device structure and can make it difficult to avoid differential color aging, WOLEDs with a single emitter are extensively investigated. In this instance, white light is generated from the combination of the emissions from the monomers of electroluminescent species and their aggregates. While WOLEDs using a single fluorescent emitter which can form excimers have also been examined,[5] most devices rely on phosphorescent molecules which can exploit light emission not only from singlet excitons, but from triplet excitons as well due to efficient intersystem crossing.[6,7]

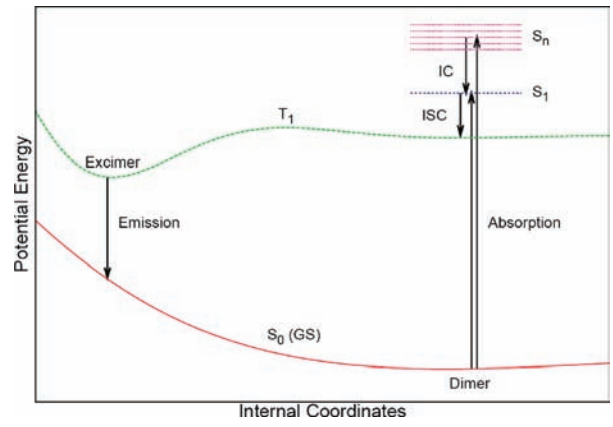

Figure 1. Schematic diagram of the relationship between a dimer of phosphor in the ground state (S_0) and an excimer in the excited state. IC denotes internal conversion from higher singlet excited states (S_n) to the lowest one (S_1) and ISC intersystem crossing from S_1 state to T_1 state.

In this context, Pt(II) compounds have been very much studied due to their square-planar geometries that offer the possibility of strong intermolecular interactions via intimate Pt−Pt contacts. In addition, these compounds often form excimers in solution or in the solid state at moderate concentrations and the aggregate emissions occur at a significantly lower energy with respect to the monomer emission (see sketch in Figure 1). In general, the emissions in Pt(II) monomers are characterized as either ligand-centered $^3\pi-\pi^*$ transitions[8] or metal-to-ligand charge-transfer (^{3}MLCT) transitions;[9] the excimer emissions are ascribed mainly to metal−metal-to-ligand charge-transfer (^{3}MMLCT) transitions[10,11]

(1) Tang, C. W.; VanSlyke, S. A. *Appl. Phys. Lett.* **1987**, *51*, 913.
(2) Burroughes, J. H.; Bradley, D. D. C.; Brown, A. R.; Marks, R. N.; Mackay, K.; Friend, R. H.; Burn, P. L.; Holmes, A. B. *Nature* **1990**, *347*, 539.
(3) Friend, R. H.; Gymer, R. W.; Holmes, A. B.; Burroughes, J. H.; Marks, R. N.; Taliani, C.; Bradley, D. D. C.; Dos Santos, D. A.; Brédas, J.-L.; Lögdlund, M.; Salaneck, W. R. *Nature* **1999**, 397.
(4) (a) D'Andrade, B. W.; Forrest, S. R. *Adv. Mater.* **2004**, *16*, 1585. (b) Misra, A.; Kumar, P.; Kamalasanan, M. N.; Chandra, S. *Semicond. Sci. Technol.* **2006**, *21*, R35–R47.

or to transitions involving $\pi-\pi$ interactions between the ligands.[11,12] We recall that an excimer is formed via the stabilization of a dimer structure in the excited state at a geometry for which the intermolecular interactions are repulsive in the ground state (Figure 1). Therefore, it is expected that the geometric structure of the excimer is significantly different from that of the dimer in the ground state; it has been shown that diplatinum compounds can display enhanced Pt−Pt interactions with shortening of the Pt−Pt distance upon excitation.[13] Unfortunately, the characterization of the excited-state geometry of an aggregate remains a very difficult experimental task; as a result, most of the studies devoted to excimers have been carried out on the basis of the crystal structures which in fact are rather associated with the ground state. An example is given by the Pt(II) (2-(4′,6′-difluorophenyl)pyridinato-*N*,$C^{2'}$)(2,4-pentanedionato-*O*,*O*) (FPt1) compound, which has been incorporated in WOLEDs as a single emitter.[6] While its excimer emission has been traced back to an ^{3}MMLCT transition due to Pt−Pt bimetallic interactions,[14−16] the crystal structures of FPt1 derivatives show no clear signs of Pt−Pt interactions while moderate ligand-based $\pi-\pi$ interactions (with ligand interplanar separations of around 3.5 Å) are observed.[17,18] This scarcity of data calls for a theoretical study of the nature and structure of phosphorescent Pt(II) excimers.

While experimental investigations of the photophysical, photochemical, and/or electrochemical properties of Pt(II) compounds and their excimers have been reported,[8–12,15,16,19] only few theoretical studies have been published.[20] In addition, theoretical studies on excimers[21−26] have been limited to relatively simple organic molecular systems such as benzene or naphthalene dimers; even in these instances, most of the investigations have relied on semiempirical methods. However, due to a lack of reliable parameterizations, semiempirical methods are generally not applicable to the study of phosphors with heavy-metal elements. Only recently have time-dependent density functional theory (TDDFT)[23] and high-level *ab initio* methods such as CASPT2[24,25] been successfully applied to the investigations of the singlet excimers in benzene and cytosine dimers. Since TDDFT remains computationally tractable for large systems and has been shown to reproduce well the transition energies of phosphorescent Pt[20] and Ir compounds,[27] this method appears as a reasonable choice to study excimer formation in organic phosphors.

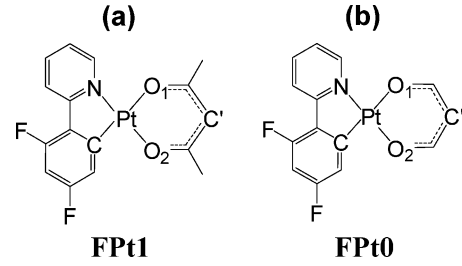

Figure 2. Structures of the Pt(II) compounds and ligands studied in this work: (a) platinum(II)(2-(4′,6′-difluorophenyl)pyridinato-*N*,$C^{2'}$)(2,4-pentanedionato-*O*,*O*) (FPt1); and (b) platinum(II)(2-(4′,6′-difluorophenyl)pyridinato-*N*,$C^{2'}$)(1,3-propanedionato-*O*,*O*) (FPt0); the *dfppy* ligand is the ligand on the left-hand side; the *acac* is on the right-hand side of FPt1; the *bdk* (*β-diketonate*) is on the right-hand side of FPt0.

Here, we investigate the FPt1[6] and FPt0 phosphorescent compounds (see Figure 2 for chemical structures) using the DFT/TDDFT methods. We first focus on the description of the monomers. We then evaluate the conditions leading to the formation of an excimer in the FPt0 dimer while keeping the monomer structures frozen; we have chosen the FPt0 compound to do so, because we wish to evaluate the respective impact of the Pt−Pt interactions and ligand−ligand interactions, without having to deal with the additional complexity due to the steric hindrance related to the methyl groups of the *acac* ligands. Finally and importantly, we discuss complete geometry optimizations of the FPt1 excimer in its T_1 state for two limiting configurations. While we are aware of the limitations of our theoretical approach, we are confident that our results provide a useful semiquantitative understanding of excimer formation

(5) (a) Tsai, M.-L.; Liu, C.-Y.; Hsu, M.-A.; Chow, T. J. *Appl. Phys. Lett.* **2003**, *82*, 550. (b) Mazzeo, M.; Vitale, V.; Sala, F. D.; Anni, M.; Barbarella, B.; Favaretto, L.; Sotgiu, G.; Cingolani, R.; Gigli, G. *Adv. Mater.* **2005**, *17*, 34. (c) Liu, Y.; Nishiura, M.; Wang, Y.; Hou, Z. *J. Am. Chem. Soc.* **2006**, *128*, 5592.
(6) (a) D'Andrade, B. W.; Brooks, J.; Adamovich, V.; Thompson, M. E.; Forrest, S. R. *Adv. Mater.* **2002**, *14*, 1032. (b) Adamovich, V.; Brooks, J.; Tamayo, A.; M., A. A.; Djurovich, P. I.; D'Andrade, B. W.; Adachi, C.; Forrest, S. R.; Thompson, M. E. *New J. Chem.* **2002**, *26*, 1171. (c) Williams, E. L.; Haavisto, K.; Li, J.; Jabbour, G. E. *Adv. Mater.* **2007**, *19*, 197.
(7) Cocchi, M.; Kalinowski, J.; Virgili, D.; Fattori, V.; Develay, S.; Williams, J. A. G. *Appl. Phys. Lett.* **2007**, *90*, 163508.
(8) Blanton, C. B.; Murtaza, Z.; Shaver, R. J.; Rillema, D. P. *Inorg. Chem.* **1992**, *31*, 3230.
(9) Balashev, K. P.; Puzyk, M. V.; Kotlyar, V. S.; Kulikova, M. V. *Coord. Chem. Rev.* **1997**, *159*, 109.
(10) (a) Kunkely, H.; Vogler, A. *J. Am. Chem. Soc.* **1990**, *112*, 5625. (b) Buchner, R.; Cunningham, C. T.; Field, J. S.; Haines, R. J.; McMillin, D. R.; Summerton, G. C. *J. Chem. Soc., Dalton Trans.* **1999**, 711.
(11) Bailey, J. A.; Hill, M. G.; Marsh, R. E.; Miskowski, V. M.; Schaefer, W. P.; Gray, H. B. *Inorg. Chem.* **1995**, *34*, 4591.
(12) Miskowski, V. M.; Houlding, V. H. *Inorg. Chem.* **1989**, *28*, 1529.
(13) (a) Rice, S. F.; Gray, H. B. *J. Am. Chem. Soc.* **1983**, *105*, 4571. (b) Kim, C. D.; Pillet, S.; Wu, G.; Fullagar, W. K.; Coppens, P. *Acta Crystallogr., Sect. A* **2002**, *58*, 133. (c) Novozhilova, I. V.; Volkov, A. V.; Coppens, P. *J. Am. Chem. Soc.* **2003**, *125*, 1079. (d) Ozawa, Y.; Terashima, M.; Mitsumi, M.; Toriumi, K.; Yasuda, N.; Uekusa, H.; Ohashi, Y. *Chem. Lett.* **2003**, *32*, 62. (e) Yasuda, N.; Uekusa, H.; Ohashi, Y. *Bull. Chem. Soc. Jpn.* **2004**, *77*, 933. (f) Stoyanov, S. R.; Villegas, J. M.; Rillema, D. P. *J. Phys. Chem. B* **2004**, *108*, 12175.
(14) D'Andrade, B.; Forrest, S. R. *Chem. Phys.* **2003**, *286*, 321.
(15) Ma, B.; Li, J.; Djurovich, P. I.; Yousufuddin, M.; Bau, R.; Thompson, M. E. *J. Am. Chem. Soc.* **2005**, *127*, 28.
(16) Ma, B.; Djurovich, P. I.; Garon, S.; Alleyne, B.; Thompson, M. E. *Adv. Funct. Mater.* **2006**, *16*, 2438.
(17) Brooks, J.; Babayan, Y.; Lamansky, S.; Djurovich, P. I.; Tsyba, I.; Bau, R.; Thompson, M. E. *Inorg. Chem.* **2002**, *41*, 3055.
(18) Cho, J.-Y.; Bomercq, B.; Barlow, S.; Suponitsky, K. Y.; Li, J.; Timofeeva, T. V.; Jones, S. C.; Hayden, L. E.; Kimyonok, A.; South, C. R.; Weck, M.; Kippelen, B.; Marder, S. R. *Organometallics* **2007**, *26*, 4816.
(19) Ma, B.; Djurovich, P. I.; Thompson, M. E. *Coord. Chem. Rev.* **2005**, *249*, 1501.
(20) (a) Klein, A.; Van Slageren, J.; Zalis, S. *Inorg. Chem.* **2002**, *41*, 5216. (b) van Slageren, J.; Klein, A.; Zalis, S. *Coord. Chem. Rev.* **2002**, *230*, 193. (c) Klein, A.; Van Slageren, J.; Zalis, S. *Eur. J. Inorg. Chem.* **2003**, *2003*, 1917.
(21) (a) Azumi, T.; McGlynn, S. P. *J. Chem. Phys.* **1964**, *41*, 3131. (b) Azumi, T.; Armstrong, A. T.; McGlynn, S. P. *J. Chem. Phys.* **1964**, *41*, 3839. (c) Azumi, T.; McGlynn, S. P. *J. Chem. Phys.* **1965**, *42*, 1675. (d) Chandra, A. K.; Lim, E. C. *J. Chem. Phys.* **1968**, *48*, 2589. (e) Chandra, A. K.; Lim, E. C. *J. Chem. Phys.* **1968**, *49*, 5066. (f) Minn, F. L.; Pinion, J. P.; Filipescu, N. *J. Phys. Chem.* **1971**, *75*, 1794. (g) Chandra, A. K.; Lim, E. C. *Chem. Phys. Lett.* **1977**, *45*, 79. (h) East, A. L. L.; Lim, E. C. *J. Chem. Phys.* **2000**, *113*, 8981. (i) de Sainte Claire, P. *J. Phys. Chem. B* **2006**, *110*, 7334.
(22) Malar, E. J. P.; Chandra, A. K. *Theor. Chim. Acta* **1980**, *55*, 153.
(23) Amicangelo, J. C. *J. Phys. Chem. A* **2005**, *109*, 9174.
(24) Olaso-Gonzalez, G.; Roca-Sanjuan, D.; Serrano-Andres, L.; Merchan, M. *J. Chem. Phys.* **2006**, *125*, 231102.
(25) Rocha-Rinza, T.; De Vico, L.; Veryazov, V.; Roos, B. O. *Chem. Phys. Lett.* **2006**, *426*, 268.
(26) Vala, M. T.; Hillier, I. H.; Rice, S. A.; Jortner, J. *J. Chem. Phys.* **1966**, *44*, 23.
(27) Hay, P. J. *J.Phys. Chem. A* **2002**, *106*, 1634.

in Pt-based organic phosphors that can help with the design of new efficient phosphors for WOLED applications.

2. Computational Methodology

Recently, Amicangelo conducted a computational investigation of excimer formation in the benzene dimer with DFT/TDDFT.[23] We note that the results were not explicitly corrected for the basis set superposition error (BSSE) on the premise that the corrections to the ground-state and excited-state energies are similar, and thus, the BSSE correction would hardly affect the excimer characterization. Amicangelo obtained results in quantitative as well as qualitative agreement with both experiment and high-level *ab initio* CASPT2 calculations with BSSE correction.[25] The successful use of DFT to describe the excimer formation in a benzene dimer can be rationalized in the following way. While traditional DFT methods are not able to describe accurately the dispersion interactions, provided that (i) the contribution of the dispersion interactions to the total interaction energies of the clusters in their ground state is quantitatively similar to that in the excited state[22] and (ii) the excimer formation can be ascribed mainly to exciton resonance,[22] then the energy differences between those states can be expected to be reliably evaluated at the DFT level. Since the Pt(II) compounds studied in this work are significantly larger than benzene, and the application of high-level *ab initio* methods would be computationally prohibitive, the choice of DFT/TDDFT methods is thus reasonable.

We employ the B3LYP exchange-correlation functional[28] which has been successfully applied for the calculation of various Ir compounds[27,29] and the benzene excimer.[23] We use the LANL2 relativistic effective core potential (RECP) and the LANL2DZ basis set for Pt and the 6-31+G* basis set for all other atoms (we note that we also tested another RECP and basis set reported in ref 30 for Pt and obtained virtually the same results for the monomer calculations;[31] therefore, we only report here the results obtained with the LANL2DZ RECP and basis set). All the calculations were conducted with the TURBOMOLE package.[32]

First, we optimized the geometries of both FPt1 and FPt0 molecules in the ground state (S_0) and the lowest triplet excited state (T_1) at the B3LYP/LANL2DZ/6-31+G* level with restricted closed-shell DFT for S_0 and unrestricted open-shell DFT for T_1. Then, using the same exchange-correlation functional, RECP, and basis sets, we constructed the potential energy surfaces (PES) of the ground state and triplet excited states of the FPt0 dimer by performing single-point DFT or TDDFT calculations for various dimer structures while keeping the monomers in their ground-state optimized geometry. In the case of cofacial configurations of the dimer, the geometry variables include the interplanar distance between monomers, the rotational angle along the Pt−Pt binuclear axis, and displacements along the axes perpendicular to the binuclear axis, see Figure 3. The PES for several additional dimer structures taken from the crystal structures of FPt1 analogues were also characterized.

Then, to evaluate the geometry modifications taking place on the individual molecules in the course of excimer formation, we performed complete geometry optimizations of some representative dimers in their T_1 excited state and ground state. To optimize the T_1 excited-state dimer structures (which, as we will discuss, are driven by Pt−Pt bimetallic interactions), we kept the same level of theory as for the monomer calculations. However, in the case of the ground-state geometry optimizations (which are highly dependent on dispersion interactions), we utilized the DFT-D methodology[33,34] with the meta-GGA exchange-correlation functional TPSS;[35] this technique successfully describes the dispersion interactions via addition of an empirical damping function and exhibits a remarkable agreement with high-level *ab initio* calculations such as MP2 in predicting ground-state geometries. Since basis sets of at least triple-ζ quality are recommended,[34] we used the TZVP basis sets and the default RECP[30] implemented in TURBOMOLE for the Pt atom. To compensate for the increase in computational requirements, we took advantage of the efficient "resolution of the identity" (RI) approximation where the four-index two-electron integrals are approximated with linear combinations of three-index integrals by employing auxiliary basis sets.[36]

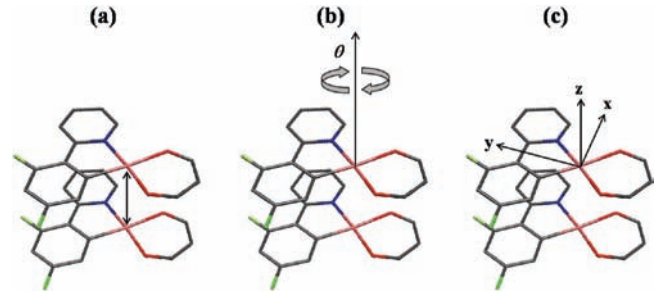

Figure 3. Representative geometry variables considered in the characterization of the dimer potential energy surfaces: (a) interplanar separation between the monomers; (b) rotational angle of one monomer with respect to the other along the Pt−Pt axis (taken as the *z*-axis); the rotational angle, θ, is referenced with respect to the perfectly cofacial configuration; (c) displacements of one of the monomers along the axes perpendicular to the Pt−Pt axis (*x*- and *y*-axes); the displacements in the direction of the depicted vectors are taken as positive.

To better understand the photophysical (excitation/emission) properties of the systems under study, we also performed natural transition orbital (NTO)[37] analyses. The NTOs are obtained as the pair of orbitals that describe at best the pair of hole and electron wave functions involved in the excitation or emission process; thus, they are a good indicator of where the electron and hole are located and help in the determination of the nature of the transition.[38] They are evaluated via the singular value decomposition of the one-particle transition density matrix, **T**, which corresponds to a $N_{occ} \times N_{virt}$ rectangular matrix (N_{occ}, number of occupied orbitals; N_{virt}, number of virtual orbitals):

$$[\mathbf{U}^{\dagger}\mathbf{T}\mathbf{V}]_{ij}| = \sqrt{\lambda_i}\delta_{ij}$$

where **U** and **V** are the square unitary transformation matrices of dimensions $N_{occ} \times N_{occ}$ and $N_{virt} \times N_{virt}$, respectively; $\mathbf{U}^{\dagger}$ is the conjugate transpose of matrix **U**; λ_i denotes the square of the singular value of matrix **T**; and δ_{ij} is the Kronecker delta. The usefulness of an NTO analysis resides in its capability of providing a clearer picture of the electronic transitions than when relying

(28) Note that we employed B3LYP functional which is compatible with that in GAUSSIAN program.
(29) Avilov, I.; Minoofar, P.; Cornil, J.; De Cola, L. *J. Am. Chem. Soc.* **2007**, *129*, 8247.
(30) Andrae, D.; Häuβermann, U.; Dolg, M.; Stoll, H.; Preuβ, H. *Theor. Chim. Acta* **1990**, *77*, 123.
(31) For instance, at the T_1 optimized geometry of FPt1, the HOMO-LUMO energy gap is calculated with the RECP and basis set of ref 30 to be 3.64 eV, which is identical to the LANL2DZ result, and the differences for the triplet excitation energies are less than 0.05 eV.
(32) (a) Bauernschmitt, R.; Ahlrichs, R. *Chem. Phys. Lett.* **1996**, *256*, 454. (b) Bauernschmitt, R.; Ahlrichs, R. *Chem. Phys. Lett.* **1997**, *264*, 573. (c) Furche, F.; Ahlrichs, R. *J. Chem. Phys.* **2002**, *117*, 7433; TURBOMOLE version 5.9.
(33) (a) Grimme, S. *J. Comput. Chem.* **2004**, *25*, 1463. (b) Grimme, S. *J. Comput. Chem.* **2006**, *27*, 1787.
(34) (a) Jurečka, P.; Černý, J.; Hobza, P.; Salahub, D. R. *J. Comput. Chem.* **2007**, *28*, 555. (b) Černý, J.; Jurečka, P.; Hobza, P.; Valdes, H. *J. Phys. Chem. A* **2007**, *111*, 1146.
(35) Tao, J.; Perdew, J. P.; Staroverov, V. N.; Scuseria, G. E. *Phys. Rev. Lett.* **2003**, *91*, 146401.
(36) Feyereisen, M.; Fitzgerald, G.; Komornicki, A. *Chem. Phys. Lett.* **1993**, *208*, 359.
(37) (a) Martin, R. L. *J. Chem. Phys.* **2003**, *118*, 4775. (b) Batista, E. R.; Martin, R. L., Natural transition orbitals. In *Encyclopedia of Computational Chemistry*, Schleyer, P. v. R., Allinger, N. L., Clark, T., Gasteiger, J., Kollman, P. A., Schaefer, H. F. I., Schreiner, P. R., Eds.; John Wiley: Chichester, U.K., 2004.

Table 1. Comparison of Selected Geometric Parameters between Theory and Experiment

	FPt1		FPt0			
geometry	S_0	T_1	S_0	T_1	expt.[a]	expt.[b]
R(Pt−N) (Å)	2.02	1.99	2.02	2.03	1.98, 2.01	2.02
R(Pt−C) (Å)	1.98	1.95	1.98	1.98	1.95, 1.98	2.00
R(Pt−O_1) (Å)	2.15	2.15	2.16	2.13	2.06, 2.08	2.07
R(Pt−O_2) (Å)	2.04	2.06	2.05	2.03	2.00, 1.99	2.06
<(N−Pt−C) (deg)	81.3	82.6	81.4	81.4	81.7, 80.9	81.4
<(O_1−Pt−O_2) (deg)	90.4	90.3	91.1	90.6	92.3, 92.3	90.8
ϕ(Pt−O_1−O_2−C′) (deg)	180.0	180.0	180.0	161.0		

[a] X-ray crystallographic data of Platinum(II) (2-(2′-thienyl)pyridinato-N,$C^{3'}$)(2,2,6,6-tetramethyl-3,5-heptanedionato-O,O).[17] [b] X-ray crystallographic data of Platinum(II) (2-phenylpyridinato-N,$C^{2'}$)(3-(5-bicyclo[2.2.1]hept-5-en-2-ylpentyl)pentane-2,4-dionato-O,O).[18]

simply on pairs of frontier molecular orbitals (FMOs). We note that, since λ_i corresponds to the contribution of a given pair of hole−electron NTOs to the overall electronic transition, the sum of all λ_i should be 1.[39] In addition, to measure the contributions of the metal d orbitals to the NTO pairs, we also conducted a Löwdin population analysis.[40]

3. Results and Discussion

3.1. Monomers of FPt1 and FPt0. The comparison between theory and experiment for several selected geometry parameters involving the Pt atom is reported in Table 1. Although the compounds studied experimentally slightly differ from those investigated here, the calculated geometries are in very good agreement with the experimental values of platinum(II) (2-phenylpyridinato-N,$C^{2'}$)(3-(5-bicyclo[2.2.1]hept-5-en-2-ylpentyl)pentane-2,4-dionato-O,O)[18] (compound **10** in Figure 4), with differences lower than 0.1 Å in bond lengths and 2° in bond angles. In the ground state, both FPt1 and FPt0 are coplanar with C_s symmetry. The two methyl substituents on the *acac* ligand are seen to have little effect on the geometry around the Pt atom, which also explains the good agreement with the experimental values of similar compounds.

The photophysical properties and energies of the frontier MOs (FMOs) of FPt1 and FPt0 are collected in Table 2 and in Table S1 (see Supporting Information), respectively, and their FMOs are displayed in Figure 5. The emission transition energies from several triplet excited states at the T_1 optimized geometries are also shown in Table S2. In the ground-state geometry, the energy gaps between the highest occupied MO (HOMO) and the lowest unoccupied MO (LUMO), $\Delta E_{(\mathrm{LUMO-HOMO})}$, of FPt1 and FPt0 are nearly the same (3.95 and 4.01 eV, respectively). This is consistent with the similar transition energies for both Pt(II) compounds; in particular, the lowest triplet excitation energies from S_0 to T_1 are nearly identical, 2.76 and 2.77 eV. The theoretical values for the $S_0 \rightarrow S_1$ transition (3.24 and 3.29 eV for FPt1 and FPt0, respectively) compare well with the lowest experimental absorption bands of 3.18 eV for FPt1[17] and 2.99 eV for compound **10** in Figure 4.[18] Upon T_1-state geometry optimization, the adiabatic T_1 emission energies are calculated to correspond to 2.78 eV in FPt0 and 2.68 eV in FPt1; the FPt1 value is in excellent agreement with the experimental data, 2.63−2.80 eV.[14,16,17,19]

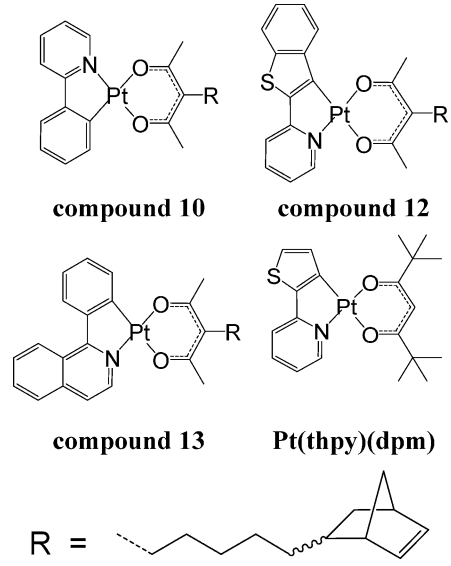

Figure 4. Structures of the Pt(II) compounds for which the crystal structures are reported in the literature. Compound **10**, platinum(II) (2-phenylpyridinato-N,$C^{2'}$)(3-(5-bicyclo[2.2.1]hept-5-en-2-ylpentyl)pentane-2,4-dionato-O,O); compound **12**, platinum(II) (2−2′-(4′,5′-benzothienyl)pyridinato-N,$C^{3'}$) (3-(5-bicyclo[2.2.1]hept-5-en-2-ylpentyl)pentane-2,4-dionato-O,O); compound **13**, platinum(II) (1-phenylisoquinolinato-N,$C^{2'}$) (3-(5-bicyclo-[2.2.1]hept-5-en-2-ylpentyl)pentane-2,4-dionato-O,O); Pt(thpy) (dpm), platinum(II) (2-(2′-thienyl)pyridinato-N,$C^{3'}$) (2,2,6,6-tetramethyl-3,5-heptanedionato-O,O). See ref 17 for Pt(thpy)(dpm) and ref 18 for compounds **10**, **12**, and **13**.

The NTO analysis provides an interesting rationalization of the geometric features in the Pt(II) compounds. The contribution of the Pt 5d orbitals in FPt1 to the pair of NTOs associated with the $S_0 \rightarrow T_1$ excitation amounts to 19.9% for the hole part and 3.5% for the electron part; those related to the $T_1 \rightarrow S_0$ emission are calculated to be 4.2% for the electron part and 14.3% for the hole part (Tables 2 and S2). Although the electronic transitions can still be characterized as ^{3}MLCT for excitation/emission, the contribution of the metal 5d orbitals to the HOMOs are estimated to be significantly smaller than in Ir compounds[27] and the amount of 5d orbital contribution does not markedly change upon excitation/emission (∼10−16%).

3.2. Dimers of Pt-Based Phosphors.

3.2.1. Characterization of Potential Energy Surfaces without Monomer Geometric Relaxation: FPt0 Dimer. We are now discussing several simple dimer structures in which the geometries of the monomers are kept frozen. These dimer

(38) See Figure S1 in Supporting Information for the comparison between the conventional analysis based on frontier molecular orbitals and NTO analysis.

(39) The effect of de-excitation in TDDFT calculations usually makes the sum of the λ_i terms to exceed 1 and the particular way of normalization of the method[39a] prevents one from performing a simple renormalization. However, since we are essentially interested in the relative importance of each NTO hole-electron pair and the effect of de-excitation is often negligible, we simply renormalized the λ_i values such that their sum becomes unity and use these readjusted values in this study. (a) Stratmann, R. E.; Scuseria, G. E.; Frisch, M. J. *J. Chem. Phys.* **1998**, *109*, 8218.

(40) (a) Löwdin, P.-O. *J. Chem. Phys.* **1950**, *18*, 365. (b) Löwdin, P.-O. *Adv. Quantum Chem.* **1970**, *5*, 185.

Table 2. Photophysical Parameters Related to the Excited States of Pt(II) Compounds (TDDFT Calculations Based on the Ground-State Geometry)

	E (eV)	*f*[a]	main excitations[b]	contributions of Pt 5d orbital to hole → electron NTOs[c]
			FPt1	
			Singlet	
S_1 ($^1A'$)	3.24	0.0282	H,H-1 → L	45.2(45.3) → 3.8(7.3)
S_2 ($^1A''$)	3.49	0.0029	H-2 → L	72.8(81.0) → 4.0(6.6)
S_3 ($^1A'$)	3.53	0.0697	H-1,H → L	39.7(40.2) → 3.5(7.0)
S_4 ($^1A'$)	3.84	0.0492	H → L + 1	43.5(43.5) → 1.1(1.2)
			Triplet	
T_1 ($^3A'$)	2.76		H-1,H → L	19.9(20.0) → 3.5(6.2)
T_2 ($^3A'$)	2.98		H → L + 1,L H-1 → L + 1,L	17.8(18.3) → 2.0(2.8)
T_3 ($^3A'$)	3.06		H,H-1 → L H,H-1 → L+1	33.5(33.8) → 4.0(6.6)
T_4 ($^3A''$)	3.36		H-2 → L	72.2(80.6) → 4.3(10.0)
			FPt0	
			Singlet	
S_1 ($^1A'$)	3.29	0.0293	H,H-1 → L	43.6(43.6) → 3.5(7.2)
S_2 ($^1A''$)	3.54	0.0030	H-2 → L H-1 → L	72.9(81.2) → 3.7(6.3)
S_3 ($^1A'$)	3.60	0.0459	H → L + 1 H → L	42.1(42.4) → 2.7(5.8)
S_4 ($^1A'$)	3.74	0.0672	H → L + 1 H-1 → L	45.0(45.0) → 3.0(3.6)
			Triplet	
T_1 ($^3A'$)	2.77		H-1,H → L	16.7(16.8) → 3.2(5.9)
T_2 ($^3A'$)	2.82		H-1,H → L + 1	11.7(12.4) → 2.4(2.5)
T_3 ($^3A'$)	3.10		H,H-1 → L	42.6(42.6) → 3.9(7.6)
T_4 ($^3A''$)	3.41		H-2 → L	72.3(80.7) → 4.0(9.9)

[a] Oscillator strength. [b] H and L denote HOMO and LUMO, respectively. [c] All the values are in %; the values between parentheses represent the total contributions of all Pt valence orbitals (5d, 6s, and 6p) to the hole and electron NTOs.

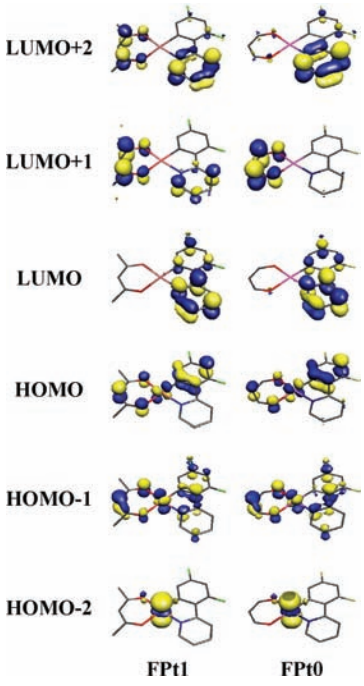

Figure 5. Frontier molecular orbitals of the Pt(II) compounds in the ground-state geometry.

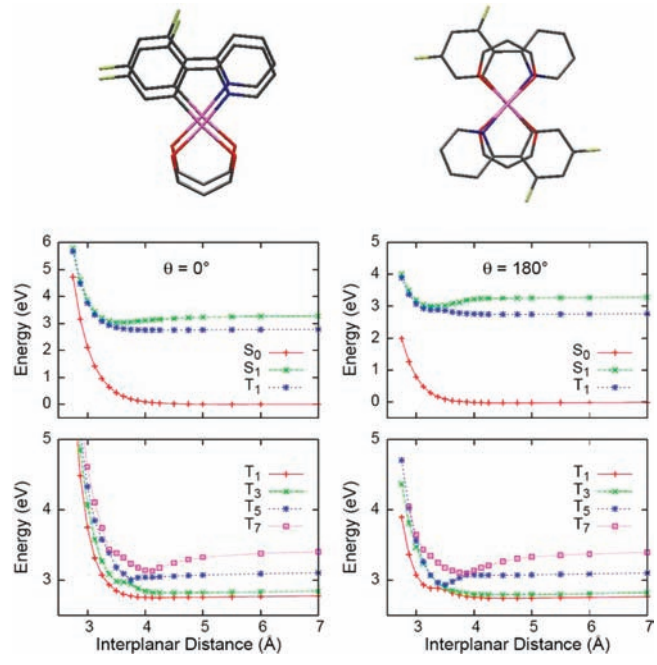

Figure 6. Sketch of the molecular structures and plot of the potential energy surfaces for the cofacial FPt0 dimers in the S_1 state and several T states (the S_0 curves are provided for the sake of reference). The zero of energy corresponds to the ground state dimer at infinite separation. (Note that, in this and subsequent figures, the state ordering is considered independently at each distance).

configurations allow us to uncover the main structural parameters impacting the dimer electronic properties and excimer formation.

3.2.1.1. Superimposed Dimers in the syn- (θ = 0°) and anti- (θ = 180°) Configuration. The PES for the cofacial FPt0 dimers with syn (θ = 0°) and anti (180°) configurations are displayed in Figure 6 as a function of Pt−Pt distance. The S_1 state presents potential wells at short intermolecular separations in both dimer structures. In contrast to the benzene dimer where the singlet excimer forms with a perfect cofacial structure,[23,25,26] the S_1

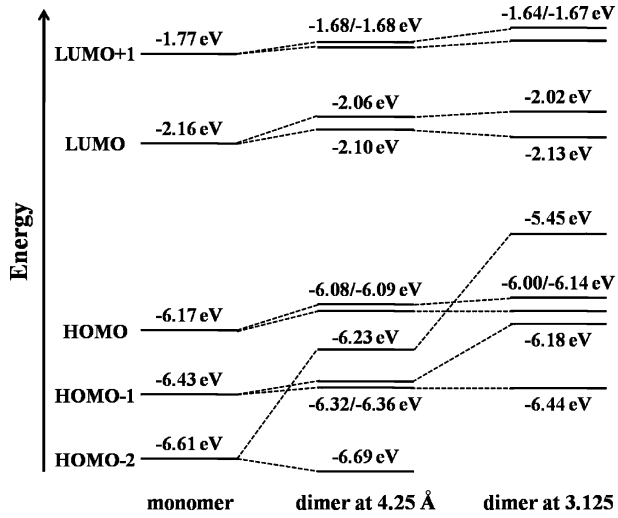

Figure 7. Influence of the intermolecular interactions on the energies of the frontier molecular orbitals of the FPt0 anti dimer at long (4.25 Å) and short (3.125 Å) Pt−Pt distances.

potential well for the syn dimer with respect to the situation at infinite spacing (stabilization by ∼0.21 eV at 3.375 Å) is relatively shallow, while the anti dimer represents a somewhat stronger excimer at similar spacing (∼0.29 eV at 3.25 Å). Thus, it appears that the interaction between the *dfppy* groups or between the *bdk* (*beta*-diketonate) ligands does not lead to singlet excimers, which suggests that another type of interaction is mainly responsible for the excimer formation in the FPt0 dimer. The T_1 PES for the anti dimer displays a very shallow well around 3.25 Å (only ∼2 meV deep with respect to the barrier), while there is no indication of excimer formation in the T_1 state of the syn dimer. We note that, unlike the FPt0 dimer, the anti configuration of the FPt1 dimer (with frozen monomer structures) does not provide for a bound T_1 state; this highlights that the steric hindrance arising from the methyl groups of the FPt1 *acac* ligands screens the other interactions associated with excimer formation (Figure S2 in Supporting Information). This is the reason why, as far as PES determinations are concerned, we have chosen to focus on the FPt0 dimer even though it is not a system that has been widely experimentally studied.

To gain more insight into the local minimum of the T_1 PES, we constructed the PES of higher triplet states for both dimer structures (Figure 6). In the anti configuration, as the intermolecular separation decreases, the T_7 state becomes increasingly stabilized, crosses the PES of other triplet excited states, and finally develops into the most stable triplet excited state. In this dimer configuration, the emission energy difference between monomer and excimer is estimated to be only ∼0.18 eV, which is significantly smaller than the experimental estimates (0.56−0.80 eV).[14] In addition, by comparing with the dimer triplet energy at infinite separation, the activation energy barrier of excimer formation is calculated to be 0.14 eV, which is about 4 times larger than the experimental value (∼37 meV).[14] In the syn dimer, the PES of the higher triplet states exhibit the same trends, but the T_7 state is not sufficiently stabilized to lead the excited dimer into an excimer, which might be related to a stronger repulsion between *dfppy* ligands than between *dfppy* and *bdk* ligands.

Figure 7 depicts the influence of the intermolecular interactions on the FMO energies of the anti dimer as a function of intermolecular separation. At a moderate spacing (4.25 Å), the interaction between the HOMO-2s of the FPt0 molecules, which correspond to the metal d_z^2 orbitals (Figure 5), is already substantial and the

Table 3. Representative Natural Transition Orbitals (NTOs) Associated with Excimer Formation of the FPt0 anti Dimer at Long (4.25 Å) and Short (3.125 Å) Pt−Pt Distances

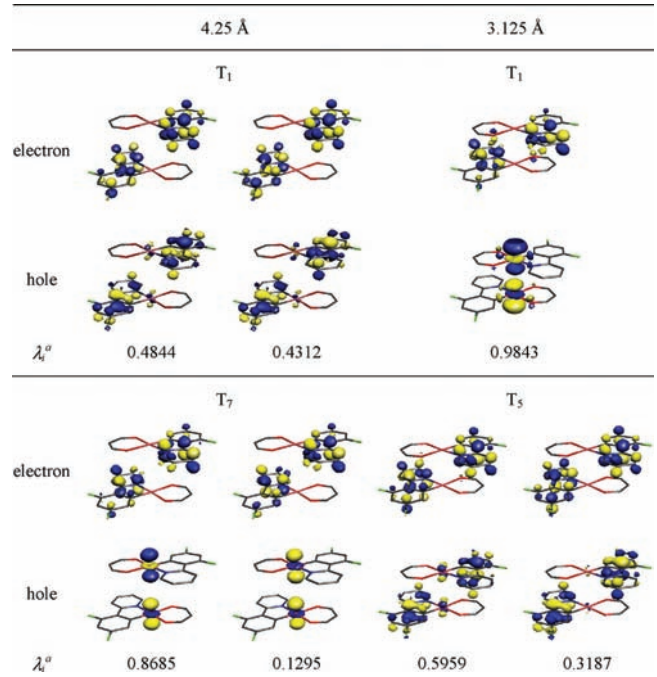

[a] λ_i denotes the square of the singular value of the transition density matrix.

energy splitting between the bonding and antibonding d_z^2 MOs amounts to 0.46 eV. At shorter intermolecular separations, this interaction increases up to the point that the antibonding d_z^2 MO now becomes the HOMO of the dimer (it lies more than 0.5 eV above the HOMO-1 at an intermolecular distance of 3.125 Å). In contrast, the dimer LUMOs remain only little affected, even at the interplanar distance of 3.125 Å.

Thus, the excimer formation observed in the anti dimer mainly originates in the Pt−Pt interactions. In agreement with previous experimental studies,[10,11] the NTO analysis of the anti dimer correlates the excimer state with an ^{3}MMLCT transition, see Table 3. While at intermediate separation (4.25 Å) the dimer T_1 excitation is reminiscent of the monomer (^{3}MLCT or ligand centered $\pi-\pi^*$ transition), at short separation, it converts to a transition between the Pt−Pt d_z^2 antibonding orbital (hole NTO) and an *dfppy* ligand-centered orbital (electron NTO); this transition is related to the T_4 transition of the monomer and the T_7 excitation of the dimer at long intermolecular distance. This picture is fully consistent with the PES plots of Figure 6.

3.2.1.2. Translation along the *x*- and *y*-Axes of the syn and anti Dimers. The effect of the displacement of one monomer with respect to the other (Figure 3) is also worth exploring in order to better characterize the interplay between the Pt−Pt bimetallic interactions and other types of interactions such as the interligand $\pi-\pi$ interactions. The PES for displacements along the *x*- and *y*-axes in the anti dimer are displayed in Figure 8. Any excimer binding disappears for displacements ≥1.0 Å regardless of the translational direction. We note that the local minima are not located at zero displacement but around 0.25 and −0.25 Å for the translations along the *x*- and *y*-axes, respectively.

When turning to the syn dimer, the PES for the T_1 state is least repulsive in the case of zero displacement. The local minimum in the excited state corresponding to the ^{3}MMLCT transition is also found for zero displacement (Figure 9);

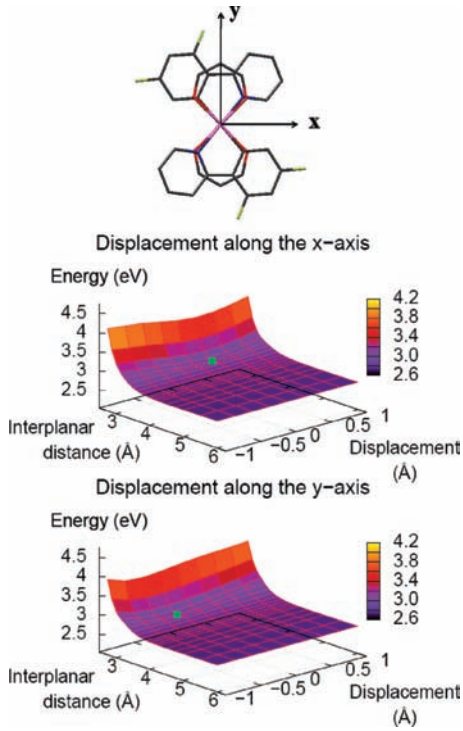

Figure 8. Potential energy surfaces for the anti dimer of FPt0 as a function of the interplanar distance and displacement along the axes perpendicular to the Pt−Pt axis. The displacements are referenced to the dimer configuration depicted at the top. Positive displacements are indicated by the axis vectors. The green points on the surfaces denote the local minima.

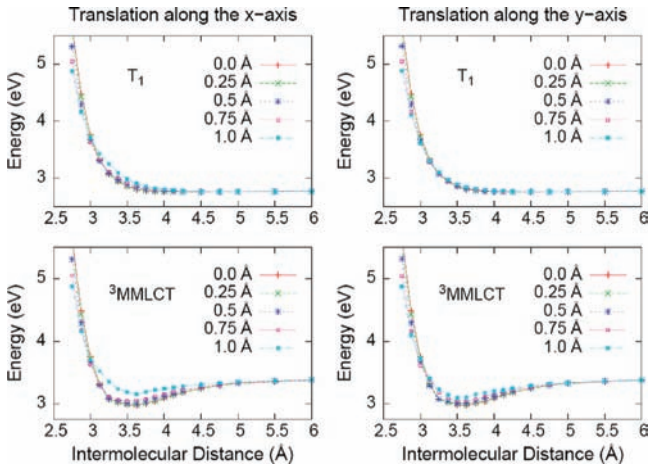

Figure 9. Potential energy surfaces (PES) for the syn dimer of FPt0 for translations along the *x*- and *y*-axes. The top panels depict PES corresponding to the T_1 state and the bottom panels display those corresponding to the ^{3}MMLCT state. See also Figure 3.

however, the PES remains nearly isoenergetic for translations less than 0.75 Å along the *x*-axis and ≤1.0 Å along the *y*-axis.

These results can be explained on the basis of the interplay between the Pt−Pt bimetallic interactions and the interligand $\pi-\pi$ interactions. In the context of the NTO analysis, while the former plays a critical role in the excimer formation via the marked destabilization of the hole NTO of the dimer, the latter also contributes by determining the stabilization of the electron NTO. In the syn dimer, the interligand $\pi-\pi$ interactions behave in a complex way. On the one hand, the electron NTO is characterized by a bonding interaction between orbitals on the difluorophenyl rings of adjacent *dfppy* ligands (Figure 10);

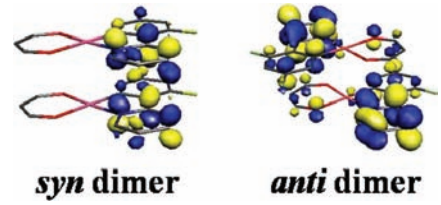

Figure 10. Electron natural transition orbitals for the syn and anti dimers of FPt0 at the interplanar distance of 3.125 Å.

therefore, a displacement in this dimer structure reduces the MO interactions and the ensuing destabilization of the electron NTO causes a reduction in the binding strength of the excimer; in addition, such a displacement weakens the strength of the bimetallic interaction. On the other hand, at short intermolecular distances, the $\pi-\pi$ interactions result in a stronger repulsion when the monomers perfectly overlap,[41] which undermines the impact of the electron NTO stabilization. We also note that the local minimum of the ^{3}MMLCT state is located at an interplanar distance around 3.5 Å, which is longer than the optimal distance of the Pt−Pt bimetallic interaction for excimer formation; this indicates that at short intermolecular distances the strong $\pi-\pi$ repulsion dominates the other interactions, including the Pt−Pt bimetallic interactions. This repulsion, however, is alleviated as one molecule of the dimer translates. Hence, overall, for displacements <0.75 Å, these opposite effects somewhat compensate each other and the PES remains nearly flat.

In the anti dimer, at the interplanar distance of the excimer state, the interligand MO interaction is in part characterized as antibonding between the chelating C atom in the difluorophenyl ring of one monomer and a chelating O atom in the *bdk* ligand of its neighbor (Figure 10). This antibonding interaction lifts up the electron NTO energy and can be avoided with a positive displacement along the *x*-axis or a negative translation along the *y*-axis. However, since such displacements also reduce the Pt−Pt bimetallic interactions, the optimal shift is limited to ca. 0.25 Å.

3.2.1.3. Rotations along the Pt−Pt Axis. Several stable dimer structures are obtained by rotating one of the molecules along the Pt−Pt bimetallic axis.[42] Among those, Figure 11 displays the dimer structures for rotational angles $\theta = 15$, 76, and 135° and the related PES; those configurations correspond to three different types of representative interligand $\pi-\pi$ interactions: displaced $\pi-\pi$ interactions between the *dfppy* ligands and between the *bdk* ligands (15°), cofacial $\pi-\pi$ interactions between the difluorophenyl and pyridine rings of the *dfppy* ligands (76°), and displaced $\pi-\pi$ interactions between the difluorophenyl rings of the *dfppy* ligands and the *bdk* ligands (135°).

In the $\theta = 15°$ dimer, the excited state corresponding to T_7 at large intermolecular distances becomes the T_1 excited state at around 3.5 Å. Although this does not result in a potential well, it does give rise to a cusp in the T_1 state, which was absent in the PES for the syn dimer. As the rotational angle increases, the potential well of the excimer emerges and becomes more prominent. For instance, in the case of the 135° dimer, the excimer state is only 50 meV higher than the monomer T_1

(41) Sinnokrot, M. O.; Sherrill, C. D. *J. Phys. Chem. A* **2006**, *110*, 10656.
(42) Various dimer structures have been obtained by rotating one of the Pt (II) molecules by 15° from 0 to 180°. Unfortunately, however, because of the triplet state stability issue, PES only for the dimers of $\theta = 15$, 30, 76, 90, and 135° in addition to the syn and anti dimers are successfully characterized. In lieu of the $\theta = 75°$ dimer, the 76° one where pyridine- and difluorophenyl-ring are optimally superimposed is used.

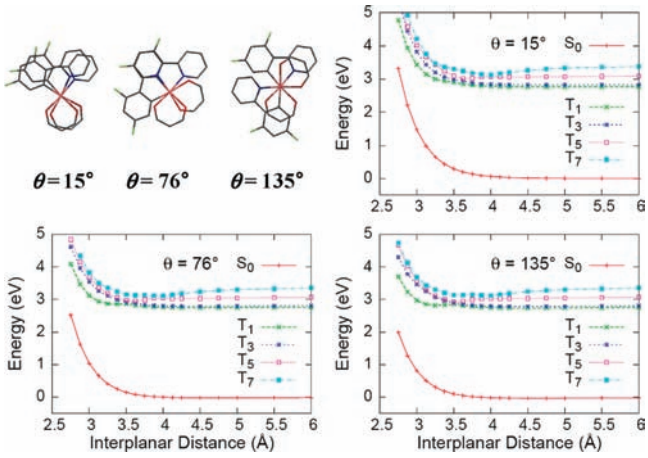

Figure 11. Molecular structures of various rotated FPt0 dimers and their potential energy surfaces for the ground state and representative triplet states.

excited state and ~30 meV deep with respect to the barrier. In addition, the ground-state PES of the 135° dimer are relatively less repulsive than those of the other dimer structures. As a result, the magnitude of the shift in the phosphorescence of excimer with respect to that of monomer increases to ~ 0.27 eV (which is ca. 0.09 eV larger than in the anti dimer).

Thus, we note that as θ increases and the strength of the $\pi-\pi$ interactions is expected to weaken, the potential well of the excimer state becomes deeper. In parallel, the ground-state PES show a similar trend; as θ increases, the PES become less repulsive, which is likely due to the relaxation of the strong repulsive forces in the $\pi-\pi$ interactions at short intermolecular distances.[41] This observation is also consistent with the conclusion drawn from the PES for the syn and anti dimers in the previous section.

3.2.1.4. Dimer Structures Built from Literature Data. D'Andrade and Forrest[14] stated that the crystal structures of FPt1 derivatives exhibit Pt−Pt bimetallic interactions and that an excited dimer, that is, an excited species at the same geometry as the ground-state dimer (Figure 1), is possibly responsible for the substantial red-shift in phosphorescence of FPt1. To the best of our knowledge, however, there has been no report to date of crystal structures of the FPt1 compound explicitly showing Pt−Pt interactions. On the other hand, the crystal structures of analogues or derivatives of FPt1 (Figure 4) have been recently reported;[17,18] however, the crystallographic data do not demonstrate any obvious Pt−Pt interactions. Hence, on the basis of such crystal structures, it is worth investigating further FPt0 dimers and evaluating the possibility of excimer formation and/or of excited-dimer structures responsible for the lowering of the emission energy.

The molecular structures of various FPt0 dimers extracted from crystal structure data and their PES are shown in Figure 12. In the displaced dimer structure (left column in Figure 12), π stacking interactions are observed between the *bdk* ligand of one molecule and the *dfppy* ligand of its neighbor. This structure is similar to that found in the crystal of compound **10** in ref 18. The second dimer structure (central column in Figure 12) serves as an example of $\pi-\pi$ interactions between the cyclometalated ligands (*dfppy*) of adjacent molecules. In the crystal structures which display interactions of this type, that is, Pt(thpy)(dpm) [thpy = 2-(2′-thienyl)pyridinato-$N,C^{3'}$; dpm = 1,3-di-*tert*-butyl-1,3-propandionato-O,O][17] and compound **12** in ref 18 Platinum(II) (2−2′-(4′,5′-benzothienyl)pyridinato-$N,C^{3'}$) (3-(5-bicyclo[2.2.1]hept-5-en-2-ylpentyl)pentane-2,4-dionato-O,O), a ligand is displaced with respect to its neighbor. However, keeping in mind that the benzene dimer favors displaced π stacking or T-shape $\pi-\pi$ interactions in the ground state[41,43] but forms an excimer at the cofacial configuration,[23,25,26] a dimer structure where the ligand π rings are cofacially superimposed was chosen for the investigation of excimer formation. In the third structure (right column in Figure 12), which is inspired by the crystal structure of compound **13** (Platinum(II) (1-phenylisoquinolinato-$N,C^{2'}$)(3-(5-bicyclo[2.2.1]hept-5-en-2-ylpentyl)pentane-2,4-dionato-O,O)) in ref 18, the Pt atoms reside on the center of one of the π rings of adjacent *dfppy* ligand. The idea behind this structure is to explore the possibility of excimer formation due to interactions between the metal d_{z^2} orbitals and ligand π orbitals.

We underline that all these dimers do not present Pt−Pt bimetallic interactions. The calculated PES indicate that none of these structures are likely to form an excimer in the lowest triplet excited state. The triplet excited states above T_1 are also consistently repulsive, except for T_7 which is slightly attractive but far from being effective in transforming the excited dimer into an excimer. Thus, these results confirm the importance of the role played by Pt−Pt bimetallic interactions in excimer formation.

3.2.2. Optimization of the Excimer T_1 State of FPt1 and FPt0. The results obtained thus far point out that the Pt−Pt bimetallic interactions are crucial to form a triplet excimer and the emission from the excimer can be traced to a ^{3}MMLCT transition; also, they imply that the interactions between ligands participate in the determination of the dimer PES in the T_1 state. However, the shifts in phosphorescent emission energy calculated for the structures investigated above are significantly smaller than the experimental value (0.18 vs 0.56−0.80 eV). A likely cause for this discrepancy is the neglect of monomer geometric relaxations in constructing the dimer PES. In addition, if we turn to FPt1, the impact of the methyl groups of the *acac* ligand on the relaxed geometry is of interest as well.

When relaxing the monomer geometries, it would be prohibitive to try and calculate the PES by taking into account all degrees of freedom. Therefore, we have chosen to fully optimize the T_1 and S_0 states in the cases of the syn and anti dimers. The respective optimized geometries of the FPt1 and FPt0 dimers are depicted in Figures 13 and S3 while representative geometric parameters and phosphorescent emission energies for the FPt1 and FPt0 dimers are listed in Tables 4 and S4, respectively.

The geometric relaxation in the T_1 state involves a couple of noteworthy deformations, that is, shortening of the Pt−Pt distance and bending of each monomer. In the absence of monomer geometry relaxation, the PES illustrated in Figure 6 for FPt0 indicate a triplet excimer formation at an interplanar separation of ca. 3.25 Å for the anti dimer, while no excimer is found for the syn dimer. When the monomer geometries in the FPt1 excimer are allowed to relax, the Pt−Pt distances in the bound T_1 state are calculated to be 2.93 and 2.92 Å for the syn and anti dimers, respectively (Table 4). While a similar contraction of the Pt−Pt distance upon excitation has been also observed in the bimetallic Pt compound $[Pt_2(\mu\text{-}P_2O_5H_2)_4]^{4-}$,[13] these distances are definitely shorter than the Pt−Pt intermolecular separations found in crystals of the Pt(II) compounds (ca. 3.5 Å). Furthermore, these Pt−Pt distances are consistent with that found in the binuclear Pt compound reported by Ma et al. (2.83 Å) which exhibits a

(43) Lee, E. C.; Kim, D.; Jurečka, P.; Tarakeshwar, P.; Hobza, P.; Kim, K. S. *J. Phys. Chem. A* **2007**, *111*, 3446.

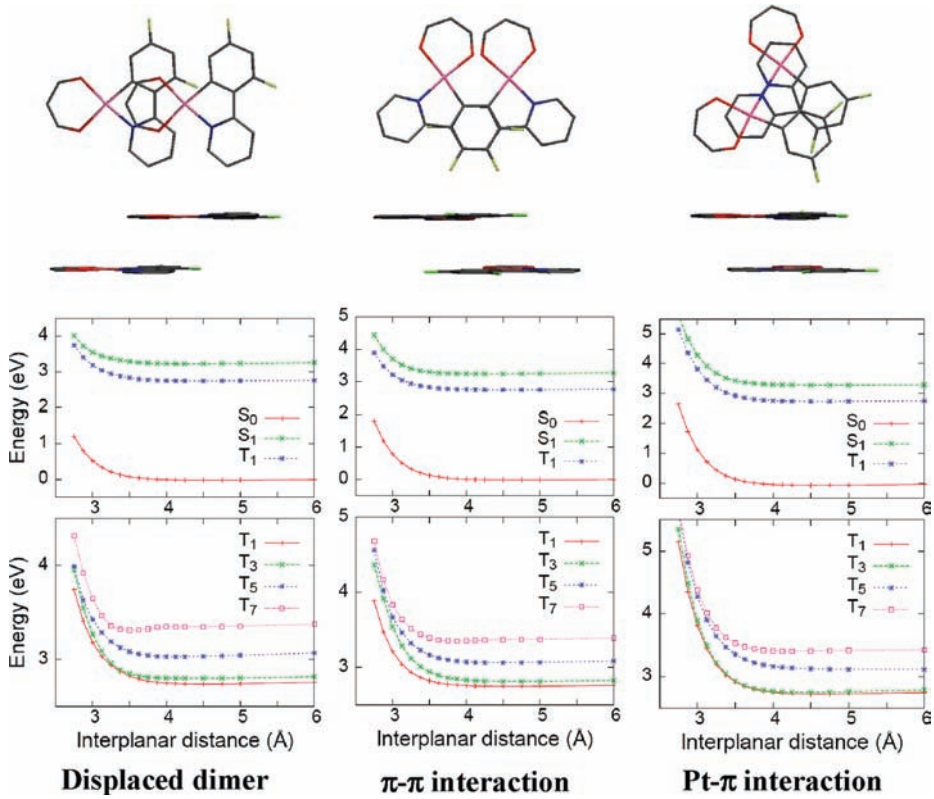

Figure 12. Molecular structures of representative dimers extracted from crystal structure data (see text for detail) and their potential energy surfaces. These FPt0 dimers do not present Pt−Pt bimetallic interactions.

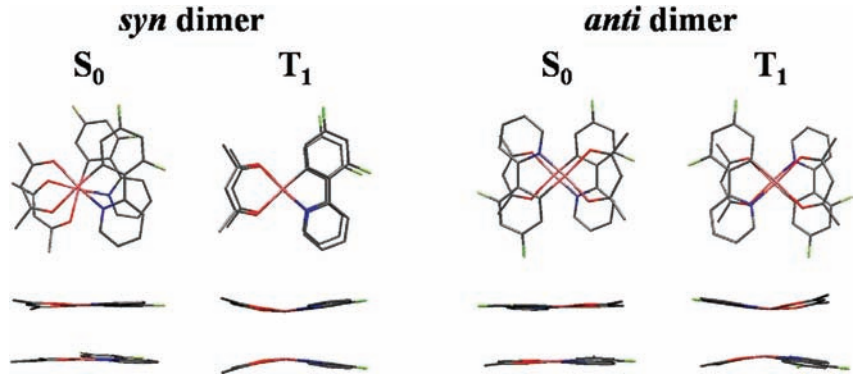

Figure 13. Top and side views of the S_0 and T_1 fully optimized geometries of the syn and anti dimers of FPt1.

significantly red-shifted phosphorescence (ca. 0.69 eV).[15,16] These geometric deformations are readily understood with the help of the NTO pictures (Table 3); in the T_1 state, the relocation of an electron from the Pt−Pt d_z^2 antibonding orbital to the *dfppy* ligand-centered orbital reduces the repulsive interaction and increases the bond order between two Pt atoms.[15] The other important geometric characteristics impacting the excimer formation are related to the interligand $\pi-\pi$ interactions. For both FPt1 and FPt0 excimers, the distances between the π-conjugated ligands are found to be in the range of 3.4−3.8 Å, that is, distances for which the repulsive forces in the $\pi-\pi$ interactions are expected to be minimal; the comparison of the relaxed dimer geometries of FPt0 and FPt1 reveals that, at these optimal interligand distances, the methyl groups of FPt1 have little impact on the geometric deformations (Tables 4 and S4). In addition, while the perfect cofacial configuration is maintained in the syn dimer, one of the molecules slides slightly with respect to the other in the anti dimer, which is consistent with the observation of the role of interligand MO interactions in the PES for monomer translations along the *x*- and *y*-axes (Figures 8 and 9). Hence, the geometric deformations of the monomers observed in both FPt1 and FPt0 excimers arise from the interplay between Pt−Pt bimetallic interactions and the interligand $\pi-\pi$ interactions.

In contrast, in the S_0 optimized geometries of FPt1 (Table 4 and Figure 13), none of the dimer structures show severe distortion of the monomer geometry, although relatively moderate Pt−Pt bimetallic interactions are observed; the monomer structures remain almost coplanar and intermolecular distances are calculated to be 3.36 and 3.37 Å for the syn and anti dimer, respectively. In both dimers, one of the molecules is parallel displaced with respect to the other by 0.17 and 0.80 Å for the syn and anti dimers, respectively, and in addition rotated along the normal axis by ∼30.9° for the syn dimer. These structures are reminiscent of the typical ground-state $\pi-\pi$ interactions,[41,43] which indicate that interligand $\pi-\pi$ interactions play an important role in the ground-state dimer structure.

Table 4. Geometric Parameters of the Optimized FPt1 Dimers in the Ground State and Lowest Triplet Excited State and Their Emission Energies

	syn dimer	anti dimer	expt.[14]
	S_0		
Interplanar separation (Å)	3.36	3.37	3.4 ± 0.1[a]
R(Pt−Pt) (Å)	3.29	3.46	
	T_1		
$E_{emission}(T_1 \rightarrow S_0)$ (eV)	1.72 (0.96)[b]	1.94 (0.74)[b]	1.83, 2.07 (0.80, 0.56)[b]
R(Pt−Pt) (Å)	2.93	2.92	
$R(\pi_\phi\text{-}\pi_\phi)$[c] (Å)	3.77		
$R(\pi_{py}\text{-}\pi_{py})$[c] (Å)	3.53		
$R(\pi_{acac}\text{-}\pi_{acac})$[c] (Å)	3.56		
$R(\pi_{acac}\text{-}\pi_{dfppy})$[d] (Å)		3.49, 3.49	
<(C′−Pt−*dfppy*)[e] (deg)	164.0, 164.0	164.0, 164.0	
ϕ(Pt−O_1−O_2−C′) (deg)	172.1, 172.1	174.4, 174.4	

[a] The experimental value corresponds to the intermolecular separation in the FPt1 dimer. See ref 14. [b] The values in parentheses denote the emission energy lowering of an excimer with respect to the monomer adiabatic emission energy. [c] The distances between the ligands are measured with respect to their center of mass. [d] In this case, for the *dfppy* ligand, its center of mass is restricted to the four central atoms, that is, the chelating N atom of the pyridine ring, the chelating C atom of the difluorophenyl ring, and two C atoms of the linkage between those two rings. [e] The angles are measured between the C′ atom of the *acac* ligand, the central Pt atom and the center of mass of the C−C linkage between the phenyl and pyridine rings of the *dfppy* ligand. See Figure 2.

The most important consequence of the geometric relaxations in the dimer T_1 state is the substantial lowering of the calculated excimer emission energy with respect to the monomer emission. The destabilized dimer HOMO at short Pt−Pt distances gives rise to a more red-shifted emission. In the syn dimer, the lowering of the calculated phosphorescent emission energy with respect to the monomer adiabatic emission is 0.96 eV, while the anti dimer exhibits a red-shifted emission by 0.74 eV; these values can be compared to experimental data in the range 0.56−0.80 eV.[14] Thus, the full geometry optimization provides for a significant enhancement of the phosphorescence energy lowering versus the one evaluated in the absence of monomer geometry relaxation (∼0.18 eV for the anti dimer).

We note that excimer emissions tend to blue-shift in more rigid environments;[15,16] since our calculations are performed in the gas phase, the calculated energy lowerings of 0.74−0.96 eV could be viewed as upper limits. We also note that the impact of the monomer geometry relaxation increases as the intermolecular distance decreases; thus, it can be expected that, if we were able to construct the PES by taking the monomer geometry relaxation into account, the overestimation of the activation energy barrier for excimer formation (calculated to be 0.140 eV vs a measured value of 0.037 eV) should be corrected.

At the short Pt−Pt distances calculated for the T_1 states of the dimers, the differences in Pt−Pt bimetallic interactions between the two dimer configurations appear to be small; the HOMO energies are calculated to be −4.95 and −4.94 eV for the syn and anti dimers, respectively. On the other hand, as seen from Figure 10, the MO interactions between ligands stabilize the LUMO of the syn dimer (−2.38 eV) to a greater extent than that of the anti dimer (−2.12 eV); the energy gap between LUMO and LUMO+1 is also substantially larger for the former (0.69 eV) than for the latter (0.19 eV). Hence, we can correlate the difference in the lowering of the phosphorescence energy between the syn and anti dimers with the interligand $\pi-\pi$ interactions.

4. Synopsis

We believe that this work represents an important step in the understanding of excimer formation in Pt-based phosphors. The main results can be summarized as follows:

(i) Pt−Pt bimetallic interactions play a critical role in the triplet excimer formation of the Pt(II) molecules and impact the red-shift in phosphorescence energy with respect to monomer emission. This is confirmed by the fact that a number of dimer configurations inspired by crystal structures of FPt1 analogues and derivatives in which Pt−Pt bimetallic interactions are absent do not lead to excimer formation.

(ii) In order for an excited dimer to develop into an excimer, its initial structure should be reasonably close to the final excimer structure (for instance, in an amorphous film)[15,16] and/or the excited state should have a sufficiently long lifetime to allow for relaxation toward the excimer structure.[14,15,19]

(iii) The interligand $\pi-\pi$ interactions do participate significantly in determining the depth of the excimer potential well and the magnitude of the shift in excimer emission energy. While the T_1-optimized geometries of the dimers exhibit short Pt−Pt distances (around 2.9 Å), the ligands distort to ensure that the interligand $\pi-\pi$ distances remain in the range of 3.4−3.8 Å, thereby minimizing the repulsive interactions.

(iv) At the T_1-optimized geometries of cofacial-type (syn and anti) FPt1 dimers, the lowerings in excimer emission energy with respect to the monomer are calculated to be 0.96 and 0.74 eV, respectively; these values correlate well with the experimental estimates. The severe geometric distortions found in the Pt(II) excimers and the significant red-shifts in phosphorescence energy stem from the interplay between the Pt−Pt bimetallic interactions and the interligand $\pi-\pi$ interactions.

Acknowledgment. This work was supported by Solvay. The authors would like to thank Dr. Veaceslav Coropceanu for many fruitful discussions. They also thank Dr. Richard L. Martin (Los Alamos National Laboratory) for help in the NTO analysis and Dr. Petr Jurečka (Academy of Sciences of the Czech Republic) for providing the DFT-D program.

Supporting Information Available: The Supporting Information collects: (i) the frontier molecular orbital energies and triplet transition energies at the T_1-state geometries for the Pt compounds studied here; (ii) the optimized geometries and energies of the monomers and dimers of FPt0 and FPt1 in the ground and lowest excited states; (iii) an illustration of the concept of natural transition orbital (NTO) analysis and a description of the NTO population analysis for the electronic transitions in FPt1. This material is available free of charge via the Internet at http://pubs.acs.org.

JA809924T